Spectral Unmixing of Pigments on Surface of Painted Artefacts Considering Spectral Variability

Yu Wang [1, 2], ShuQiang Lyu [1, 2], Bo Ning [3], Ding Yan [3], MiaoLe Hou [1, 2], PengYu Sun [1, 2], LiHong Li [3]

[1] School of Geomatics and Urban Spatial Informatics, Beijing University of Civil Engineering and Architecture, No.15 Yongyuan Road, Daxing District, Beijing, China -wydyx0705@163.com, lvshuqiang@bucea.edu.cn, houmiaole@bucea.edu.cn, 1108140023001@stu.bucea.edu.cn .
[2] Beijing Key Laboratory for Architectural Heritage Fine Reconstruction & Health Monitoring, No.15 Yongyuan Road, Daxing District, Beijing, China
[3] Yungang Academy, Datong, Shanxi Province, China -ningbo007@163.com, 752044653@qq.com, 13233616482@163.com .

Keywords: Hyperspectral Remote Sensing, Spectral Variability, Spectral Unmixing, Pigments.

Abstract

Painted artefacts, such as murals and paintings, are the treasures of human civilization. Pigment is an important component of their surfaces. It is crucial to study the composition and proportion of pigments on the surface of painted artefacts for the field of heritage conservation. In this study, hyperspectral remote sensing was used to invert the abundance of mixed pigments by spectral unmixing. Spectral variability effects are often present in hyperspectral images. Hyperspectral images of cultural artefacts also suffer from spectral variability due to factors such as particle size and impurities within the pigment, and acquisition conditions. Therefore, spectral variability was incorporated into the Linear Mixed Model of the pigment spectral unmixing. The unmixing methods are classified into two categories based on whether or not spectral libraries are used. In the experiment, computer synthesized data and laboratory-made sample blocks of mixed pigments, which mixed with different ratios of Azurite and Malachite, were selected as validation data. Five commonly used algorithms for solving the spectral variability problem, namely MESMA, Fractional Sparse SU, ELMM, RUSAL, and BCM, are used for pigment unmixing and compared with FCLS, which does not consider spectral variability. The results show that ELMM has the highest unmixing accuracy of *aRMSE* and *xRMSE* compared to other methods. At the same time, it can be seen from the metric of *SAM* that ELMM is able to extract reliable endmember variability spectral, which is more suitable for solving the problem of spectral variability in pigment unmixing. Finally, we apply ELMM to real artefacts Yungang Grottoes mural paintings, and obtain a lower *xRMSE* than FCLS, which improves the unmixing accuracy.

1. Introduction

Painted cultural artefacts such as murals and paintings are precious material cultural heritage with great artistic value and historical significance. In recent years, compositional analysis of surface pigments of painted cultural artefacts has become a research hotspot. As artefacts are not renewable, the use of non-invasive techniques has become an essential means of analysis. The typical techniques include X-ray fluorescence (XRF) and Raman spectroscopy, which can analyse pigments from a molecular and elemental point of view. For example, red pigments in historical plastics were identified through an in situ analysis method based on Raman microscopy (Angelin et al., 2021). Raman spectroscopy, XRF, and hyperspectral imaging were used to identify and map the watercolour pigments used by the eighteenth-century botanical illustrator Ferdinand Bauer (Mulholland et al., 2017). Hyperspectral technology, with its advantages of map integration and non-contact detection, is an important tool for pigment analysis. Its application in the pigment analysis of painted artefacts can obtain the spectral reflectance of pigments. And it is able to explore the pigment distribution of large area artefacts. An important direction of hyperspectral techniques for pigment analysis is the spectral unmixing of pigments, which refers to obtaining the composition and proportions of the pigments. In a hyperspectral image of a pigment, a pixel can be described as a spectrum in a mixture of several pure pigments. Pure pigment spectral can be considered as endmember (EM) and their abundance indicates the proportion of pure pigments. Many pigment unmixing methods rely on spectral unmixing techniques. These are similar to the algorithms for the unmixing of land features. The difference, however, is that the pigments on the surface of the painted artefacts are mixed in certain proportions. Its mixing is small-scale and dense, and there may be no pure pigments for hyperspectral images.

The modelling of unmixing has been studied by many scholars. Currently, the commonly used model is the linear mixed model (LMM), which has a simpler and clearer physical meaning. The surface pigments of the painting "*The Scream*" (1893) were mapped using Fully Constrained Least Squares (FCLS) to identify different proportions of pigments in the mixture, employing known endmembers (Deborah et al., 2014). The pigment unmixing of an ancient Egyptian painting was conducted using sparse unmixing by variable splitting and augmented Lagrangian (SUnSAL) (Rohani et al., 2016). Nonlinear mixing models (NLMM) have also been proposed for the research of small-scale compact mixing. The proportions of each pigment in the mineral pigment mixture were calculated using FCLS and three NLMM unmixing methods (Lyu et al., 2021).

In recent years, spectral variability has been widely proposed in spectral unmixing algorithms. The spectral characteristics of a material can vary in hyperspectral data due to a variety of reasons such as environmental, atmospheric and temporal factors, while the material may also have inherent spectral variability (Zare and Ho, 2013). Spectral variability is mainly due to atmospheric effects, illumination and topographical variations, and intrinsic variations in the spectral characteristics of materials (due to physicochemical differences) (Borsoi et al., 2021). Meanwhile, the authors in this article summarized various unmixing algorithms for solving spectral variability. Similarly, spectral variability exists in the unmixing of pigments on the surface of painted artefacts using hyperspectral techniques. As the hyperspectral images of the artefacts are usually collected indoor,

This contribution has been peer-reviewed. The double-blind peer-review was conducted on the basis of the full paper.
https://doi.org/10.5194/isprs-annals-X-4-2024-403-2024 | © Author(s) 2024. CC BY 4.0 License.

a large part of the spectral variability comes from the artefacts themselves, including the particle size within the pigment, the influence of impurities, dust on the surface, textural factors, and the influence of the collodion and the pigment carrier side of the equation. Another reason is due to the acquisition conditions, the influence of the light source and so on. Therefore, in order to improve the accuracy of pigment unmixing, it is crucial to address the issue of spectral variability. One of the main ways to address spectral variability is to consider acquiring a large library of spectral, which should theoretically contain all the potentially variable spectral for each material. Currently the main methods to solve the unmixing of spectral variability using spectral library are Multiple Endmember Spectral Mixing Analysis (MESMA) (Roberts et al., 1998) and sparse unmixing (Bioucas-Dias and Figueiredo, 2010). Most of these methods require preprocessing of the spectral library (Xu et al., 2016) or extracting the spectral library from the image for the purpose of improving the experimental accuracy and efficiency. However, the unmixing results of these methods mostly depend on the quality of the spectral library. In addition, it is difficult to obtain a large spectral library in real scenarios. Therefore, solving spectral variability without a priori knowledge of spectral library has also been of wide interest. Four spectral variability unmixing methods that do not depend on a spectral library include local unmixing methods (Goenaga et al., 2012), parametric EM models (Drumetz et al., 2016), endmember-model-free unmixing (Hong et al., 2018), and Bayesian methods (Gao et al., 2016) (Borsoi et al., 2021).

In this study, we will use two types of methods for pigment unmixing in response to the absence of pure endmembers for spectral mixing of pigments on the surface of artefacts. The first type is based on spectral libraries, including MESMA and Fractional Sparse SU. The second type is the representative method that does not use spectral libraries, named extended LMM(ELMM), robust unmixing by variable splitting and augmented Lagrangian (RUSAL), as well as beta compositional model (BCM). In addition, we compare these methods with FCLS. Computer synthesized data and laboratory-made sample blocks of mixed pigments were selected to validate the applicability of these methods to the unmixing of pigment spectral variability.

2. Methodology

First, we assumed that the spectral are mixed in a way that conforms to the LMM, and that each image endmember must satisfy the abundance non-negativity constraint (ANC) and the abundance sum to 1 constraint (ASC). The LMM model is expressed as follows:

$$\boldsymbol{x}_n = \sum_{p=1}^{P} a_{np}\boldsymbol{m}_p + \boldsymbol{\varepsilon}_n \tag{1}$$

$$a_{np} \geq 0, \sum_{p=1}^{P} a_{np} = 1 \tag{2}$$

where $\boldsymbol{x}_n$ is the hyperspectral reflectance matrix of the nth pixel in the image, P is the number of endmembers, $\boldsymbol{m}_p$ is the matrix of the pth endmember, a_{np} represents the abundance of the pth endmember in the nth pixel, and $\boldsymbol{\varepsilon}_n$ represents the noise.

2.1 Unmixing using Spectral Libraries

2.1.1 MESMA: The basic idea of the MESMA algorithm is to iteratively search for all possible combinations of endmembers in the spectral library to minimize the reconstruction error of each image endmember in the LMM model. The algorithm formula is expressed as:

$$\underset{\boldsymbol{a}_n, \boldsymbol{m}_n}{\operatorname{argmin}} \|\boldsymbol{x}_n - \boldsymbol{m}_n\boldsymbol{a}_n\|^2 \tag{3}$$

$$\boldsymbol{m}_n \in \boldsymbol{M}, \boldsymbol{a}_n \geq 0, 1^{\mathrm{T}}\boldsymbol{a}_n = 1 \tag{4}$$

where $\boldsymbol{m}_n$ represents the combination of endmembers for the iterative search, $\boldsymbol{M}$ is the ensemble of all possible endmember matrices, $\boldsymbol{x}_n$ is the reflectance matrix of the nth pixel of the hyperspectral image, and $\boldsymbol{a}_n$ is the abundance matrix of the nth pixel. The MESMA algorithm obtains the optimal solution when the reconstruction error (RE) is minimum.

2.1.2 Sparse Unmixing (SU): Another approach to unmixing with spectral variability using spectral libraries is sparse unmixing. Its basic idea is to select a small number of spectra as endmembers in the spectral library to minimize the RE of the image. The formula for sparse unmixing is expressed as:

$$\underset{\boldsymbol{a}_n \geq 0}{\operatorname{argmin}} \|\boldsymbol{x}_n - \boldsymbol{m}_{Lib}\boldsymbol{a}_n\|^2 \tag{5}$$

$$\|\boldsymbol{a}_n\|_0 \leq P, 1^{\mathrm{T}}\boldsymbol{a}_n = 1 \tag{6}$$

where $\boldsymbol{M}_{Lib}$ is the input spectral library, $\boldsymbol{x}_n$ is the reflectance matrix of the nth pixel of the hyperspectral image, $\boldsymbol{a}_n$ is the abundance matrix of the nth pixel, and P is the number of input endmembers. $\|\cdot\|_0$ is the L_0 paradigm, which calculates the number of non-zero endmembers in the vector.

When dealing with spectral variability in sparse unmixing, the inclusion of multiple spectral for each material (constituting endmember bundles) is considered, as well as the use of a sparse $L_{2,1}$ paradigm in the abundance estimation optimization problem (Drumetz et al., 2019). This method is known as fractional sparse unmixing (Fractional Sparse SU) and is used in this paper as a method to address the spectral variability of pigments.

However, when the input spectral library is very large, the algorithms for MESMA and sparse unmixing may have very high computational cost and the problem of multiple solutions. In response to the above problems, most of the methods for extracting spectral libraries in hyperspectral images are used in feature unmixing. In contrast, pure pigments may not be present on the surface of the artefacts, extracting spectral libraries from the images is not applicable. In order to solve this problem, we created a small spectral library according to the colour system of the pigments, to which we added a variety of typical pigments and included the spectral of each pigment with different painting layers and different particle sizes.

2.2 Unmixing without the use of Spectral Libraries

2.2.1 ELMM: The ELMM model serves as an extension of the LMM to account for variability effects caused primarily by changes in light. The model is shown below:

$$\boldsymbol{x}_n = \boldsymbol{M}\varphi_n\boldsymbol{a}_n + \boldsymbol{\varepsilon}_n \tag{7}$$

where $\boldsymbol{\varphi}_n$ is the multiplicative diagonal matrix, $\boldsymbol{M}$ is the endmember matrix, $\boldsymbol{a}_n$ is the abundance matrix, and $\boldsymbol{\varepsilon}_n$ is the noise matrix. The endmember spectral of each pixel are extended using $\boldsymbol{\varphi}_n$ in ELMM to account for complex spectral variability.

The solution criterion of ELMM can be expressed by the following equation:

$$J\left(\boldsymbol{A}, \underline{\boldsymbol{M}}, \boldsymbol{\Psi}\right) = \frac{1}{2}\sum_{n=1}^{N}(\|\boldsymbol{x}_n - \boldsymbol{m}_n\boldsymbol{a}_n\|_2^2 + \lambda_m\|\boldsymbol{m}_n - \boldsymbol{m}_0\varphi_n\|_F^2) + R(\boldsymbol{A}) + R(\boldsymbol{\Psi}) \quad (8)$$

All variables in Eq (8). are non-negative. where $\boldsymbol{A}$ is the abundance matrix, $\boldsymbol{M}$ is the set of endmember matrices, and $\boldsymbol{\Psi}$ is the set of scale matrices $\boldsymbol{\varphi}_n$, i.e., $\boldsymbol{M} = \{\boldsymbol{m}_n\}$ and $\Psi = \{\boldsymbol{\varphi}_n\}$. $\|\cdot\|_2$ is the L_2 paradigm and $\|\cdot\|_F$ is the F paradigm. λ_m is a parameter that controls the strength of the ELMM execution. R ($\boldsymbol{A}$) and R ($\boldsymbol{\Psi}$) are regularization terms for the abundance and scale factors, which serve to incorporate constraints on the variables and enhance spatial smoothing. It should be noted that ELMM is very sensitive to model initialization and parameter settings, so finding the right model initialization and parameters is crucial.

2.2.2 RUSAL: The RUSAL algorithm (Halimi et al., 2016) is a typical approach for the Endmember-model-free unmixing to address the effects of outliers and spectral variability in hyperspectral images. The method introduces an additional residual term in the LMM to account for spectral variability and other unmodelled effects, which can be expressed as:

$$\boldsymbol{x}_n = \boldsymbol{M}\boldsymbol{a}_n + \phi_n^{ME}(\boldsymbol{b}_n) + \varepsilon_n \quad (9)$$

where $\boldsymbol{M}$ is the endmember matrix, $\boldsymbol{a}_n$ is the abundance matrix and $\boldsymbol{\varepsilon}_n$ is the noise matrix. The additional term ϕ_n^{ME} is expressed as the product of two matrices:

$$\phi_n^{ME}(\boldsymbol{b}_n) = \boldsymbol{F}^{\mathrm{T}}\boldsymbol{b}_n \quad (10)$$

where ϕ_n^{ME} is a smooth spectral function, $\boldsymbol{F}$ denotes the Discrete Cosine Transform (DCT) matrix, which controls the sparsity of the space, and $\boldsymbol{b}_n$ is the vector coefficient of the DCT.

2.2.3 BCM: BCM (Du et al., 2014) is a type of Bayesian model. The spectral mixing in BCM is LMM and the endmembers are represented by beta distribution. The model assumes a univariate beta distribution for each endmember in each band:

$$e_{pl} \sim B(\cdot\,|\alpha_{pl}, \beta_{pl}) \quad (11)$$

where $B(\cdot)$ denotes the beta distribution, which is mathematically expressed as:

$$B(e|\alpha,\ \beta) = \Gamma(\alpha)\Gamma(\beta)\Gamma\ (\alpha+\beta)\ ^{-1} e^{\alpha-1}(1-e)^{\beta-1} \quad (12)$$

where e_{pl} denotes the reflectivity value of the pth endmember in the lth band. α_{pl} and β_{pl} denote the parameters of the beta distribution, both of which have non-negative values. Thus, each pixel is considered to be a random variable whose distribution is a convex combination of the endmember of the beta distribution:

$$x_{nl} \sim \mathbf{X}(\cdot\,|A_n, \alpha_l, \beta_l) \quad (13)$$

Where

$$\mathbf{X}(\cdot\,|A_n, \alpha_l, \beta_l) = \sum_{p=1}^{P} a_{np} B(e_{pl}|\alpha_{pl}, \beta_{pl}) + \varepsilon_{nl} \quad (14)$$

where x_{nl} denotes the reflectivity value of the lth band in the nth pixel in the image. P is the total number of endmembers, a_{np} is the abundance value of the pth endmember in the nth pixel, and ε_{nl} is the noise.

2.3 Accuracy Evaluation

In order to evaluate the performance of these algorithms for pigment unmixing, we used the overall root mean square error (*aRMSE*) of abundance and the root mean square error (*xRMSE*) of reconstruction of the image to evaluate the algorithms:

$$aRMSE = \frac{1}{N}\sum_{n=1}^{N}\sqrt{\frac{1}{P}\sum_{p=1}^{P}(a_{np_{true}} - \hat{a}_{np})^2} \quad (15)$$

$$xRMSE = \frac{1}{N}\sum_{n=1}^{N}\sqrt{\frac{1}{L}\sum_{l=1}^{L}(x_{nl_{true}} - \hat{x}_{nl})^2} \quad (16)$$

In addition, we will evaluate the endmembers obtained by the three methods MESMA, Fractional Sparse SU, and ELMM using Spectral Angle Mapping (*SAM*):

$$SAM_M = \frac{1}{LPN}\sum_{n=1}^{N}\sum_{p=1}^{P}\arccos\left(\frac{\mathbf{m}_{np}^T\hat{\mathbf{m}}_{np}}{\|\mathbf{m}_{np}\|\|\hat{\mathbf{m}}_{np}\|}\right) \quad (17)$$

3. Result and Analysis

3.1 Simulated Data

In order to compare and verify the applicability of the above methods, we selected two kinds of simulated data. The first one is computer synthesized data. Abundance data of size 50 × 50 were randomly generated in a Gaussian random field with spatial correlation added. The true abundance of the three endmember of the synthesised hyperspectral image is shown in Fig. 1. The endmembers were selected from three spectral data sets collected in the laboratory, namely Cinnabar, Malachite and Azurite, with a wavelength range of 350 nm to 2500 nm. In order to simulate the spectral variability in a real scene, we added perturbations to the endmembers spectral using the Hapke model (Hapke, 1981), as shown in Fig. 2. Moreover, in order to simulate the mixing of pigments, the abundance value of each pixel was set to less than 1 in the synthesized data (no pure image endmembers). Finally, Gaussian noise (SNR = 30) was added to the synthesized data.

The second type of simulated data is a laboratory-made sample block of mixed pigments of Azurite and Malachite, blending in different ratios (2:8, 3:7, 6:4, 5:5). Spectral images were acquired using a hyperspectral imager (THEMIS-VNIR/400H from Themis Vision System, USA) with a wavelength range of 400 nm to 1000 nm. The sample blocks of mixed pigments are shown in Table 1.

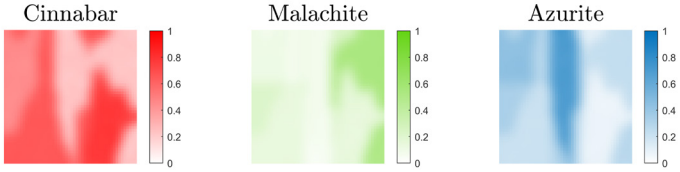

Figure 1. True abundance values of Cinnabar, Malachite and Azurite

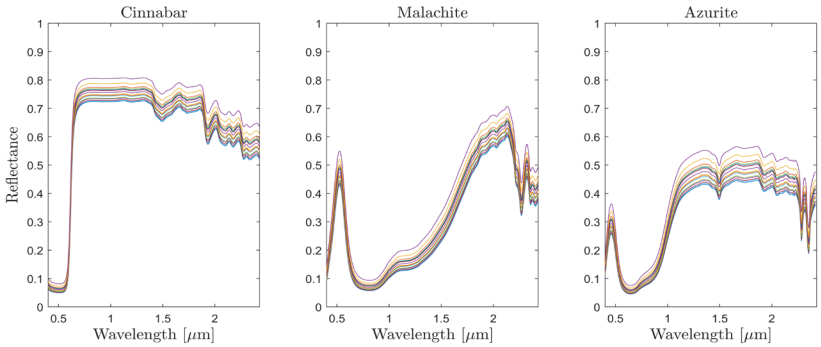

Figure 2. Spectral variability of endmember generated by the Hapke model

Azurite: Malachite	2:8	3:7	4:6	5:5
Sample blocks of mixed pigments				

Table 1. Sample blocks of pigments with different mixing ratios of Azurite and Malachite

3.2 Unmixing Results

The above two data were unmixed using six methods, FCLS, MESMA, Fractional Sparse SU, ELMM, RUSAL and BCM, with the results from the FCLS algorithm used as a preliminary abundance for the other results. The computer hardware environment for all experiments in this paper is Intel(R) Xeon(R) Sliver 4110 CPU @ 2.10Hz, 32GB RAM, Windows system, and Matlab 2023 (a) platform.

For the computer synthesized hyperspectral data, the unmixed abundance map is shown in Fig. 3. And Fig. 4 shows the variant endmember spectral obtained from the three results of MESMA, Fractional Sparse SU and ELMM (endmember variant spectral could not be obtained from RUSAL and BCM). The accuracy ratings of the six methods are given in Table 2.

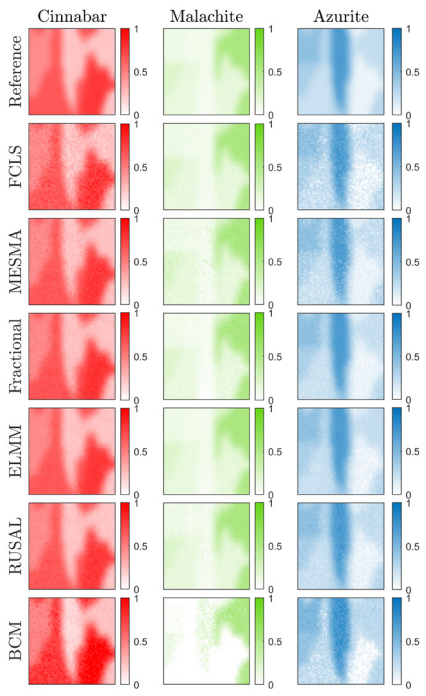

Figure 3. Pigment abundance maps from different methods

The evaluation results for the computer synthesized data show that all methods except the BCM method have a higher unmixing accuracy than the FCLS, which does not solve the spectral variability. The ELMM model has the best unmixing results for the mixed data in all three-evaluation metrics. The BCM algorithm is less effective and the reason for this may be due to the fact that it is not applicable to the data that does not have pure pixels.

Based on the results of the experiments of computer synthesized data (BCM is less suitable for pigment unmixing and has a high computational cost), the BCM method is not used on the second simulated data, which are samples of mixed pigments. Since the real samples of mixed pigments cannot represent the real spectral variability, only the *aRMSE* and *xRMSE* are used in the accuracy evaluation. The accuracy of pigment unmixing is shown in Table 3 and Table 4.

	aRMSE	*xRMSE*	SAM_M	time (s)
FCLS	0.0418	0.0182	NaN	0.4
MESMA	0.0364	0.0162	0.1155	16.68
Fractional	0.0266	0.0158	0.065	17.26
ELMM	**0.0153**	**0.0144**	**0.0328**	22.8
RUSAL	0.022	0.0147	NaN	4.26
BCM	0.1112	0.0441	NaN	1105.54

Table 2. Evaluation of the accuracy of the unmixing results of the computer synthesized data

	Azurite: Malachite				Average *aRMSE*
	2:8	3:5	4:6	5:5	
FCLS	0.0659	0.0484	0.0321	0.0491	0.0489
MESMA	0.1216	0.0932	0.0404	0.1392	0.0986
Fractional	0.1218	0.0673	0.0703	0.1652	0.1062
ELMM	**0.0593**	**0.0388**	**0.0210**	**0.0399**	**0.0397**
RUSAL	0.0413	0.0837	0.0645	0.0483	0.0594

Table 3. *aRMSE* for the samples of mixed pigments unmixing results

	Azurite: Malachite				Average *xRMSE*
	2:8	3:5	4:6	5:5	
FCLS	0.1038	0.098	0.0885	0.0849	0.0938
MESMA	0.0174	0.0183	0.0168	0.0159	0.0171
Fractional	0.0167	0.0164	0.0148	0.0137	0.0154
ELMM	**0.0007**	**0.0007**	**0.0007**	**0.0007**	**0.0007**
RUSAL	0.0048	0.0044	0.0039	0.0036	0.0042

Table 4. *xRMSE* for the samples of mixed pigments unmixing results

The results of the accuracy evaluation in Tables 3 and 4 show that for the samples of mixed pigments data, the unmixing method of ELMM is the best. The other methods, although performing well on *xRMSE*, are inferior to FCLS and ELMM for abundance estimation. we suppose that there are three reasons for this situation. The first, the input spectral libraries do not contain more spectra of the same material variability for the methods that need to use spectral libraries. The second, the spectral variability of the pigments is not fully represented by the Hapke model and a more consistent representation of the spectral variability of the pigments needs to be found. The third, the pigment mixing is small scale mixing and there is the effect of non-linear mixing factors.

ELMM is more accurate compared to other methods, and we believe there are two reasons for this. Firstly, ELMM has a corresponding scaling matrix for each pixel, so that the endmembers can be changed proportionally, which can better resist the spectral variability. Secondly, the selection of appropriate parameters to adjust the scaling degree of the scale matrix is also the key to the high accuracy of ELMM. Too little scaling of the scaling matrix is not enough to solve the spectral variability, and too much scaling will lead to large errors in the unmixing results.

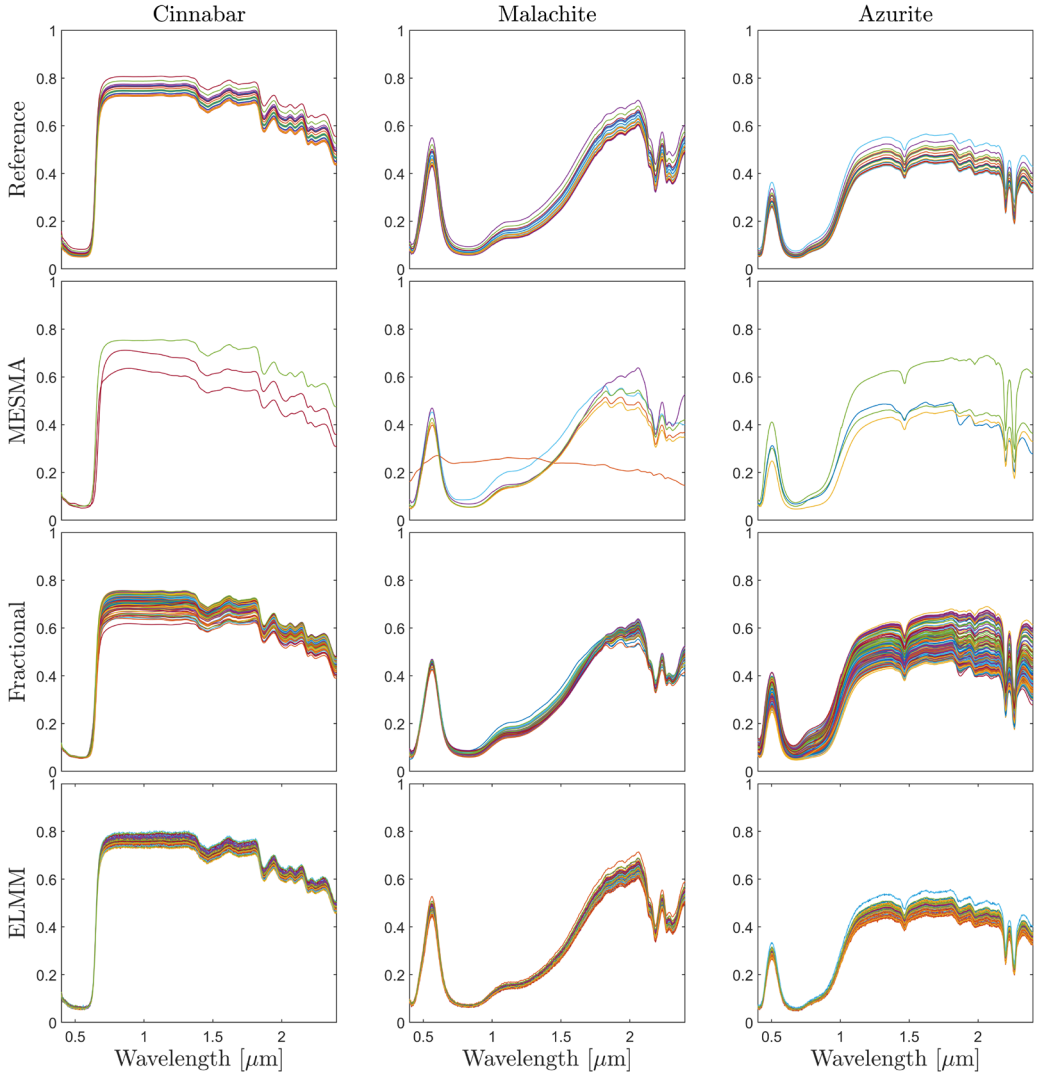

Figure 4. Spectral variability of endmember extracted using different methods

3.3 Real Mural Application

We chose the hyperspectral image collected on mural on the east wall of the sixth cave of Yungang Grottoes (Shanxi, China) as the verification data of real artefacts, as shown in Fig. 5. The several unmixing methods compared in this paper belong to supervised unmixing, which needs to obtain endmember information in advance, among which the best result is ELMM.

whereas the priori endmember information is often not available in real murals, the input endmembers of FCLS and ELMM are extracted in the image. It is also compared with the unsupervised nonnegative matrix factorization-quadratic minimum volume (NMF-QMV) method, which does not require known end endmembers (Zhuang et al., 2019). The results of the three methods are shown in Fig. 6.

Since the unmixing results of the real artefacts are unknown, only *xRMSE* is chosen for the accuracy evaluation. It is found that although NMF-QMV does not need input endmembers, it cannot make a good spectral distinction between black and green pigments. With the same input endmembers, the *xRMSE* of FCLS was 0.0411 and the *xRMSE* of ELMM was 0.0033. It can be concluded that the unmixing accuracy of ELMM is higher. Meanwhile, due to the addition of spatial constraints in ELMM, its unmixing results are smoother.

Figure 5. Hyperspectral images of mural on the east wall of Cave 6th of the Yungang Grottoes

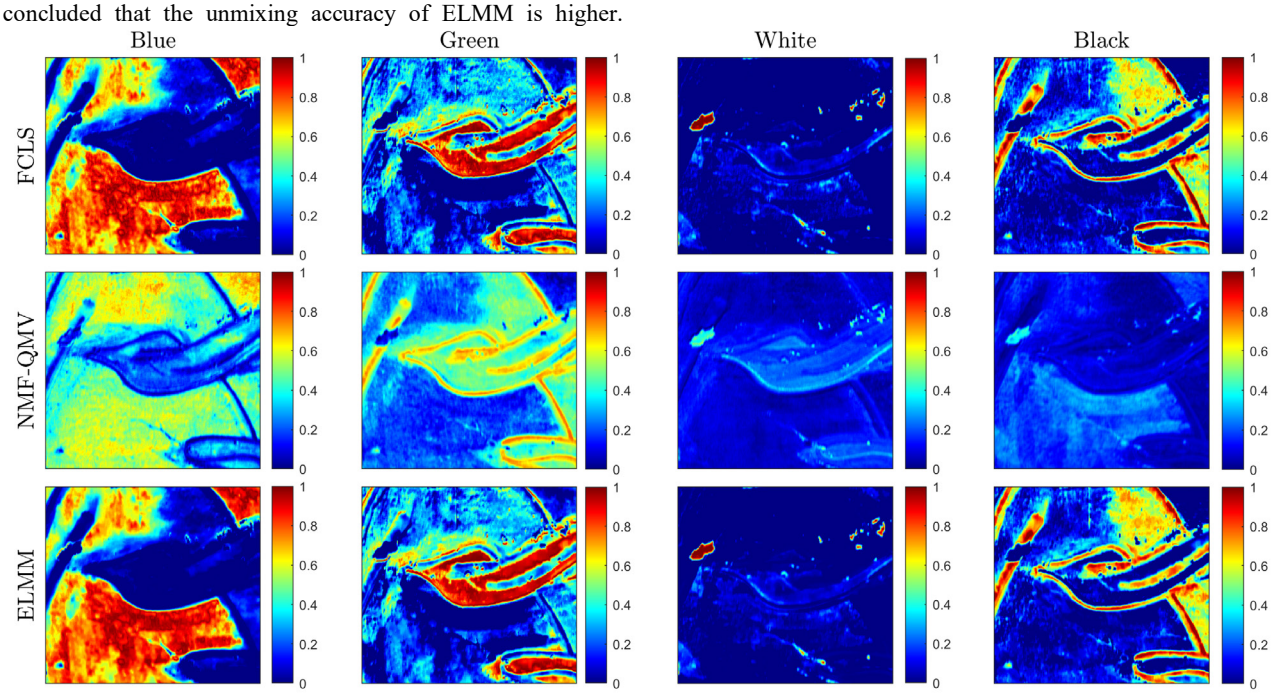

Figure 6. Abundance maps of FCLS and ELMM

4. Conclusion

In this study, we introduced the spectral variability effect in the problem of unmixing surface pigments of artefacts and analysed the spectral variability of mixed pigments. We classified the methods for solving the spectral variability into two categories based on whether the spectral libraries are used or not. Five commonly used methods, named MESMA, Fractional Sparse SU, ELMM, RUSAL, and BCM, are adopted to unmix the spectrum of mixed pigments. The *aRMSE* and *xRMSE* of simulated data and real pigment mixed samples show that the ELMM method has the highest unmixing accuracy. In addition, it is able to provide specific endmember variant spectral and the SAM_M is more accurate compared to methods using spectral libraries. However, ELMM is more sensitive to the input parameters and the initialization of the abundance matrix, and some optimization can be done for the specific initialization and parameters. Several other methods perform well on *xRMSE*, but they are less suitable for abundance estimation compared to FCLS and ELMM. Finally, we applied ELMM to unmixing of a hyperspectral image of mural in the Yungang Grottoes and obtained abundance results with higher accuracy than FCLS.

Currently, most of the methods for solving spectral variability need to obtain priori endmembers information in advance, so it is necessary to combine spectral variability unmixing with endmember extraction methods that do not rely on pure pixels in future research. Meanwhile, for such tight mixing of pigments, the mechanism of spectral variability occurring in the surface pigments of artefacts should be further understood, and the nonlinear mixing effect of the mixed pigments should be considered in the study of spectral variability in order to find a more suitable method for pigment unmixing.

Acknowledgements

This research was supported by the National K&D Program of China (No. 2022YFF0904400), National Natural Science Foundation of China (No.42171356, No.42171444).

References

Angelin, E. M., França de Sá, S., Picollo, M., Nevin, A., Callapez, M. E., Melo, M. J., 2021: The identification of synthetic organic red pigments in historical plastics: Developing an in situ analytical protocol based on Raman microscopy. *Journal of Raman Spectroscopy*, 52(1), 145-158.

Mulholland, R., Howell, D., Beeby, A., Nicholson, C.E., Domoney, K., 2017: Identifying eighteenth century pigments at

the Bodleian library using in situ Raman spectroscopy, XRF and hyperspectral imaging. *Heritage Science*, 5, 1-19.

Deborah, H., George, S., Hardeberg, J.Y., 2014: Pigment mapping of the scream (1893) based on hyperspectral imaging. //*Image and Signal Processing: 6th International Conference, ICISP 2014, Cherbourg, France, June 30 – July 2, 2014. Proceedings 6*, 247-256.

Rohani, N., Salvant, J., Bahaadini, S., Cossairt, O., Walton, M., Katsaggelos, A., 2016: Automatic pigment identification on roman egyptian paintings by using sparse modeling of hyperspectral images. //*2016 24th European signal processing conference (EUSIPCO).*

Lyu, S., Meng, D., Hou, M., Tian, S., Huang, C., Mao, J., 2021: Nonlinear mixing characteristics of reflectance spectra of typical mineral pigments. *Minerals*, 11(6), 626.

Zare, A., Ho, K.C., 2013: Endmember variability in hyperspectral analysis: Addressing spectral variability during spectral unmixing. *IEEE Signal Processing Magazine*, 31(1), 95-104.

Borsoi, R.A., Imbiriba, T., Bermudez, J.C.M., Richard, C., Chanussot, J., Drumetz, L., Tourneret, J.Y., Zare, A., Jutten, C., 2021: Spectral variability in hyperspectral data unmixing: A comprehensive review. *IEEE Geoscience and Remote Sensing Magazine*, 9(4), 223-270.

Roberts, D.A., Gardner, M., Church, R., Ustin, S., Scheer, G., Green, R.O., 1998: Mapping chaparral in the Santa Monica Mountains using multiple endmember spectral mixture models. *Remote Sensing of Environment*, 65(3), 267-279.

Bioucas-Dias, J.M., Figueiredo, M.A., 2010: Alternating direction algorithms for constrained sparse regression: Application to hyperspectral unmixing. //*2010 2nd Workshop on Hyperspectral Image and Signal Processing: Evolution in Remote Sensing.* 1-4.

Xu, M., Zhang, L., Du, B., Zhang, L., 2016: An image-based endmember bundle extraction algorithm using reconstruction error for hyperspectral imagery. *Neurocomputing*, 173, 397-405.

Goenaga, M.A., Torres-Madronero, M.C., Velez-Reyes, M., Van Bloem, S.J., Chinea, J.D., 2012: Unmixing analysis of a time series of Hyperion images over the Guánica dry forest in Puerto Rico. *IEEE Journal of Selected Topics in Applied Earth Observations and Remote Sensing*, 6(2), 329-338.

Drumetz, L., Veganzones, M.A., Henrot, S., Phlypo, R., Chanussot, J., Jutten, C., 2016: Blind hyperspectral unmixing using an extended linear mixing model to address spectral variability. *IEEE Transactions on Image Processing*, 25(8), 3890-3905.

Hong, D., Yokoya, N., Chanussot, J., Zhu, X.X., 2018: An augmented linear mixing model to address spectral variability for hyperspectral unmixing. *IEEE Transactions on Image Processing*, 28(4), 1923-1938.

Gao, L., Zhuang, L., Zhang, B., 2016: Region-based estimate of endmember variances for hyperspectral image unmixing. *IEEE Geoscience and Remote Sensing Letters*, 13(12), 1807-1811.

Drumetz, L., Meyer, T.R., Chanussot, J., Bertozzi, A.L., Jutten, C., 2019: Hyperspectral image unmixing with endmember bundles and group sparsity inducing mixed norms. *IEEE Transactions on Image Processing*, 28(7), 3435-3450.

Halimi, A., Bioucas-Dias, J.M., Dobigeon, N., Buller, G.S., McLaughlin, S., 2016: Fast hyperspectral unmixing in presence of nonlinearity or mismodeling effects. *IEEE Transactions on Computational Imaging*, 3(2), 146-159.

Du, X., Zare, A., Gader, P., Dranishnikov, D., 2014: Spatial and spectral unmixing using the beta compositional model. *IEEE Journal of Selected Topics in Applied Earth Observations and Remote Sensing*, 7(6), 1994-2003.

Hapke, B., 1981: Bidirectional reflectance spectroscopy: 1. Theory. *Journal of Geophysical Research: Solid Earth*, 86(B4), 3039-3054.

Zhuang, L., Lin, C.H., Figueiredo, M.A., Bioucas-Dias, J.M., 2019: Regularization parameter selection in minimum volume hyperspectral unmixing. *IEEE Transactions on Geoscience and Remote Sensing*, 57(12), 9858-9877.